A simple flash carbonization route for conversion of biomass to porous carbons with high CO_2 storage capacity

Edward A. Hirst, Alison Taylor, and Robert Mokaya*

School of Chemistry, University of Nottingham, University Park, Nottingham NG7 2RD, U. K.

E-mail: r.mokaya@nottingham.ac.uk (R. Mokaya)

Abstract

This work offers a new, and simpler, method for the carbonisation of biomass that involves flash carbonisation of biomass at relatively low temperature ($\leq$ 400 ^{o}C). We successfully converted the biomass precursor (eucalyptus sawdust) to carbonaceous matter via flash heating for a short period of time (5 – 10 minutes) under a flow of air. On activation, the flash carbonized carbon offers high yields of activated carbons with higher microporosity compared to sawdust derived activated carbons prepared via hydrothermal carbonization or conventional pyrolysis. Depending on the level of activation, the flash carbonized sawdust-derived activated carbons retain some 'woody' morphology preserved from the sawdust. The porosity of the carbons can be tailored towards being predominantly microporous, which generates adsorbents that exhibit very attractive CO_2 uptake (up to 5.0 mmol g^{-1}) at 1 bar and 25 ^{o}C. Moreover, depending on the level of activation, it is possible to tailor the porosity of the carbons such that they simultaneously exhibit high post-combustion (< 1 bar) and pre-combustion (20 bar) CO_2 capture capability. The carbons exhibit exceptional performance for low pressure swing adsorption (PSA) with working capacity of up to 8.3 mmol g^{-1} for a pure CO_2 stream (6 to 1 bar) and up to 5.6 mmol g^{-1} for flue gas (1.2 to 0.2 bar), while the working capacity for vacuum swing adsorption (VSA) reaches 5.3 mmol g^{-1} under pure CO_2 (1.5 to 0.05 bar), and 2.1 mmol g^{-1} for flue gas (0.3 to 0.01 bar) conditions.

1. Introduction

Porous carbons have become increasingly attractive as energy materials for many on-going attempts to find new and more sustainable methods of generating and storing energy.[1-6] Much recent research has been devoted to exploring new ways of preparing porous carbons with optimised properties that are directly targeted at energy-related applications.[2-4,6-10] One of the issues that has emerged recently is the question of the carbon balance in the synthesis of porous carbon materials. For this reason there has been increasing interest in the use of biomass-based precursors as starting materials for the preparation of porous carbons.[2,-11-18] Amongst porous carbons, one of the most versatile class are activated carbons due to their stability and variable porosity. The renewed interest in activated carbons has spurred a search for new trends in their synthesis, which are motivated by the desire to achieve one or all of the following; (i) greater sustainability, including being carbon neutral, (ii) simpler and cheaper preparation routes and/or (iii) attainment of new or improved properties for specific applications. Sustainability may be readily addressed by the use of renewable biomass (or biomass waste) as starting material, while improved properties can be achieved via careful synthesis regimes for targeted applications.

The conventional preparation of porous carbons from biomass incorporates an initial step involving either hydrothermal carbonisation (HTC)[19-22] or pyrolysis,[23-26] wherein the starting material is converted to carbon-rich carbonaceous matter prior to the activation step. The former involves thermochemical decomposition of biomass into so-called hydrochar under superheated water conditions,[19-22] while for the latter, the carbonaceous matter is generated via enrichment of carbon content during thermal treatment at elevated temperature (typically 600 – 900 ^{o}C) under oxygen-free conditions.[23-26] Both hydrothermal carbonisation and conventional pyrolysis of biomass are relatively lengthy processes (i.e., several hours) and also require either high temperatures or specialized high pressure equipment. It is therefore desirable to explore new biomass to carbon processes that may occur for much shorter periods of time (minutes) and at

much lower temperatures. Moreover, the 'green' credentials of carbons would be enhanced if they are generated via processes that are lowly energy-intensive.

Conventional pyrolysis is usually performed at 600 – 900 ^{o}C under an oxygen-free atmosphere, which results, successfully, in the removal of volatile components in the form of gaseous products and the rearrangement of residual carbon atoms into aromatic rings that form graphitic micro-crystallites.[27-31] In considering the possible use of lower temperatures for the biomass to carbon process, it is worth noting that during such high temperature pyrolysis, the evolution of volatiles (i.e., H_2O, CO_x, CH_4, and light hydrocarbons) takes place at temperature of 200 – 350 ^{o}C with hardly any mass loss above ca. 400 ^{o}C. This means that the biomass to carbonaceous matter transformation is essentially complete at ca. 400 ^{o}C. With this consideration in mind, and in an effort to simplify the carbonisation step, it would be desirable to explore pathways that would achieve similar outcomes but via processes that occur for much shorter periods of time (5 – 10 minutes) and at lower temperature ($\leq$ 400 ^{o}C) augmented by the presence of air.[32,33] Such processes, at low temperature in the presence of air, may be referred to as flash carbonisation. To the best of our knowledge there are hardly any previous reports on such flash carbonization biomass conversion, especially under atmospheric conditions. Moreover, as far as we are aware, carbonaceous matter formed from the controlled flash carbonisation of biomass in air has never been used as starting material for the preparation of activated carbon. This is an important consideration as it is well known that the nature and type of precursor carbonaceous matter plays a key role in determining the properties (e.g., porosity) of activated carbons.[34-40] A separate but equally important motivation for this study is an attempt to reproduce carbonaceous matter similar to so-called CNL1 carbon.[40] The CNL1 carbon, which yields activated carbons with unique and attractive properties with respect to packing density and gas storage capacity was obtained from accidental and uncontrolled burning of wood under fierce fire conditions.[40] In contrast the present work seeks to deliberately (i.e., via controlled and reproducible conditions and

processes) generate activated carbons with properties similar to those derived from the accidentally obtained CNL1 carbon.[40]

Sawdust is the choice of feedstock in this study as it is inexpensive and extremely widely available as an agricultural waste product.[41] The majority of sawdust waste is usually disposed of via combustion at landfill sites, and therefore finding a use for sawdust valorization would also deal with issues of disposal and reduce greenhouse gas emissions from uncontrolled combustion. Moreover, unlike directly edible biomass, the use of sawdust does not conflict with food supplies. The cost, availability and renewable nature of sawdust means it is well suited as a precursor for the preparation of activated carbons. Using sawdust as an example, we offer here a first account of the porosity generated in flash-carbonized biomass as a function of the activation conditions, namely, KOH/carbon ratio and temperature. The porosity of the resulting carbons encouraged us to explore their application as CO_2 storage materials for post-combustion capture scenarios. For context, we also provide comparisons between the flash carbonization-derived carbons and those obtained from hydrochars via hydrothermal carbonization.

2. Experimental Section

2.1 Materials

Non-homogenous sawdust from the residues of eucalyptus wood was used as the non-carbonised feedstock or starting material. The sawdust (1 – 4 g), ground into a fine powder was placed in an alumina boat and heated in a horizontal tube furnace to 400 °C under an atmosphere of nitrogen at heating ramp rate of 10 °C min^{-1}. Once at 400 °C, the sawdust was exposed to a flow of air only for 5 - 10 minutes, after which the furnace was left to cool under a flow of nitrogen gas only. The resulting carbonaceous matter was designated as ACSD (i.e., air carbonized saw dust) carbon.

For activation, the ACSD carbon and KOH were ground together into a fine powder at a KOH/carbon weight ratio of either 2 or 4, giving a homogeneous dark grey powder. The powder

was placed in an alumina boat and heated in a furnace to 600, 700 or 800 °C at a heating ramp rate of 3 °C min^{-1} under an atmosphere of nitrogen gas and held at the final temperature for 1 h, after which the sample was allowed to cool under a flow of nitrogen. The resulting activated samples were then washed with stirring in 10% HCl at room temperature, and then repeatedly washed with deionized water until neutral pH was achieved for the filtrate. The samples were then dried in an oven at 120 °C. The activated carbons were designated as ACSD-xT, where x is the KOH/carbon ratio and T is the activation temperature (in °C). Thus a carbon activated at KOH/carbon ratio of 2 and at 800 °C is designated as ACSD-2800.

2.2 Characterisation of samples

Thermogravimetric analysis (TGA) was performed using a TA Instruments SDT Q600 analyser under flowing air conditions (100 mL/min). Powder XRD analysis was performed using a PANalytical X'Pert PRO diffractometer with Cu-Kα light source (40 kV, 40 mA) with step size of 0.02° and 50 s time step. Raman spectra were recorded using a Horiba-Jobin-Yvon LabRAM Raman microscope with a 532 nm laser operating at *ca*. 4 mW (10%) and a 600 lines/mm grating. Spectra were collected by averaging 8 acquisitions of 60 s duration. The Raman shift was calibrated using the Rayleigh peak and the 520.7 cm^{-1} Si line from a Si (100) reference sample. CHN elemental analysis was performed using an Exeter Analytical CE-440 Elemental Analyser. Analysis of porosity and determination of textural properties was performed via nitrogen sorption using a Micromeritics ASAP 2020 sorptometer or Micromeritics 3FLEX sorptometer. Prior to analysis (at -196 °C), the carbon samples were degassed under vacuum at 200 °C for 12 h. Surface area was calculated using the Brunauer-Emmett-Teller (BET) method applied to adsorption data in the relative pressure (P/P_o) range of 0.02 – 0.22. The total pore volume was determined from the total nitrogen uptake at close to saturation pressure ($P/P_o \approx 0.99$). The micropore surface area and micropore volume were determined via *t*-plot analysis. Non-local density functional theory (NL-DFT) was applied to

nitrogen adsorption data to determine the pore size distribution. SEM images were recorded using an FEI Quanta200 microscope, operating at a 5 kV accelerating voltage. Transmission electron microscopy (TEM) images were obtained using a JEOL 2100F instrument operating at 200 kV equipped with a Gatan Orius CCD for imaging. The samples were suspended in distilled water and dispersed onto lacey carbon support film prior to analysis.

2.3 CO_2 uptake measurements

CO_2 uptake was determined using a Hiden Isochema Intelligent Gravimetric Analyser (IGA-003). Before CO_2 uptake measurements, the carbon samples were degassed at 200 °C under vacuum for several hours. Adsorption-desorption isotherms were measured at 25 ^oC over CO_2 pressure range of 0 – 20 bar.

3. Results and Discussion

3.1 Properties of flash air carbonised ACSD carbon

This study set out to explore a simpler route for the conversion of biomass to carbonaceous matter involving flash carbonisation. A key target of the carbonisation process is to enrich the carbon content in the resulting carbonaceous matter. We therefore determined the elemental composition of the raw sawdust and compared it to that of the ACSD carbon (Table 1). The carbon content increases following the flash carbonisation from 46.4 wt% for the sawdust to 72.4 wt% for the ACSD carbon. We note that the carbon content (72.4 wt%) of the ACSD carbon is much higher than that (57.4 wt%) of hydrochar (SD hydrochar) obtained from sawdust via hydothermal carbonisation (Table S1). The H content reduces from 5.8 wt% for sawdust to 3.2 wt% for ACSD carbon, while for SD hydrochar it remains unchanged (Table 1 and Table S1). Flash carbonisation causes the O content to reduce significantly from 47.8 wt% (raw sawdust) to 24.2 wt% for ACSD carbon, which is a much lower O content compared to 37.0 wt% for SD hydrochar. It is noteworthy that the elemental composition of the ACSD carbon is very similar to that of so-called CNL1

carbon obtained by burning of wood in air under fierce fire conditions.[40] The elemental composition of ACSD carbon and that of CNL1 carbon[40] indicate that air carbonisation of biomass yields carbonaceous matter that is rich in carbon but with relatively low amounts of O and no N.

Table 1. Elemental analysis of raw sawdust, air-carbonised sawdust-derived carbon (ACSD) and activated carbons derived from the ACSD carbon.

Sample	C [%]	H [%]	O [%]	(O/C)[a]	(H/C)[a]
Sawdust	46.4	5.8	47.8	0.773	1.500
ACSD	72.4	3.2	24.2	0.251	0.530
ACSD-2600	78.2	1.9	19.9	0.191	0.294
ACSD-2700	83.4	0.9	15.7	0.141	0.129
ACSD-2800	88.1	0.4	11.5	0.098	0.055
ACSD-4800	88.7	0.4	10.9	0.092	0.054

[a]Atomic ratio

Figure 1 shows the TGA curve for the ACSD carbon during thermal treatment to 800 ^{o}C at ramp rate of 10 ^{o}C min^{-1} under flowing air conditions. The ACSD carbon is stable up to ca. 270 ^{o}C, beyond which it burns off in a single step mass-loss event that is complete at 480 ^{o}C with virtually no residue left. The relatively wide burn off temperature range (270 – 480 ^{o}C) is consistent with the nature of the ACSD carbon, which is mainly non-graphitic (i.e., amorphous) carbon as might be expected for carbonaceous matter generated via low temperature carbonisation. Indeed the powder XRD pattern of ACSD carbon (Figure S1) exhibits two very broad features centred at 2-theta of 22^{o}, and 44^{o}, which are normally ascribed, respectively, to the (002) and (100) peaks of diffractions from graphitic domains. The very broad nature of the peaks indicates that any graphitic domains lack planarity and therefore that ACSD carbon is predominantly amorphous.

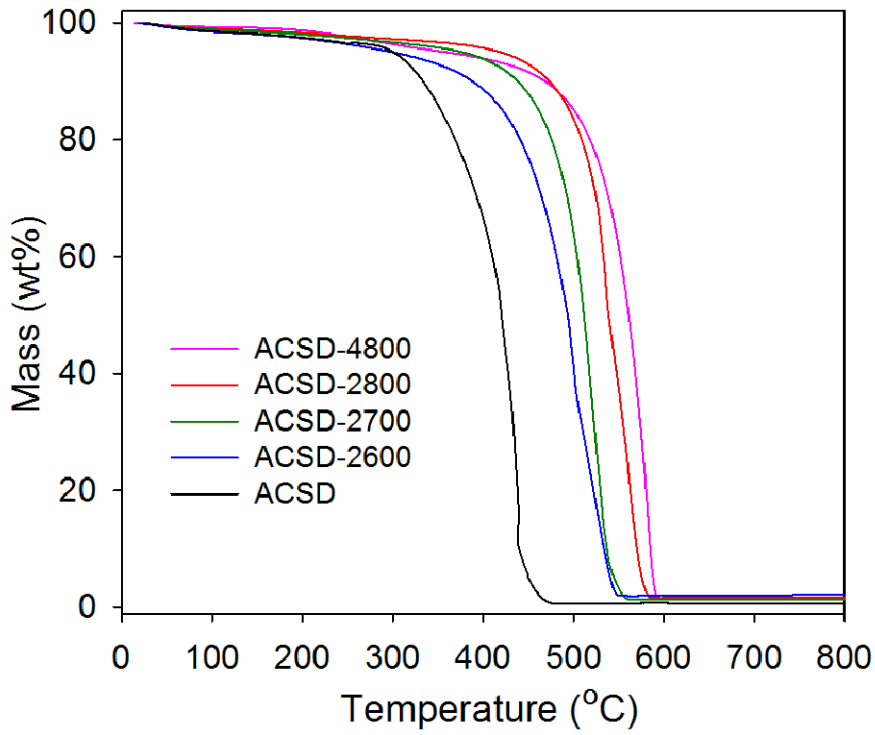

Figure 1. Thermogravimetric analysis (TGA) curve of ACSD carbon and activated ACSD-xT carbons thermally treated in air. See experimental section for sample designation.

The SEM images of the ACSD carbon (Figure 2 and Figure S2) indicate particle morphology comprising of an extended honeycomb structure. Such particle morphology, which is retained from the pre-carbonization structure of wood, is typical of chars generated from lignocellulosic biomass.[28,29,40] The flash carbonised ACSD carbon exhibits some porosity (Figure S3), and has a surface area of 127 m^2 g^{-1}, pore volume of 0.06 cm^3 g^{-1}, micropore surface area of 87 m^2 g^{-1} and micropore volume of 0.039 cm^3 g^{-1}. The level of porosity is therefore very similar to that of CNL1 carbon.[40] The pore size distribution of the ACSD carbon (Figure S3) is dominated by pores of size 5.5 Å along with a much smaller proportion of 7 Å and 12 Å pore channels.

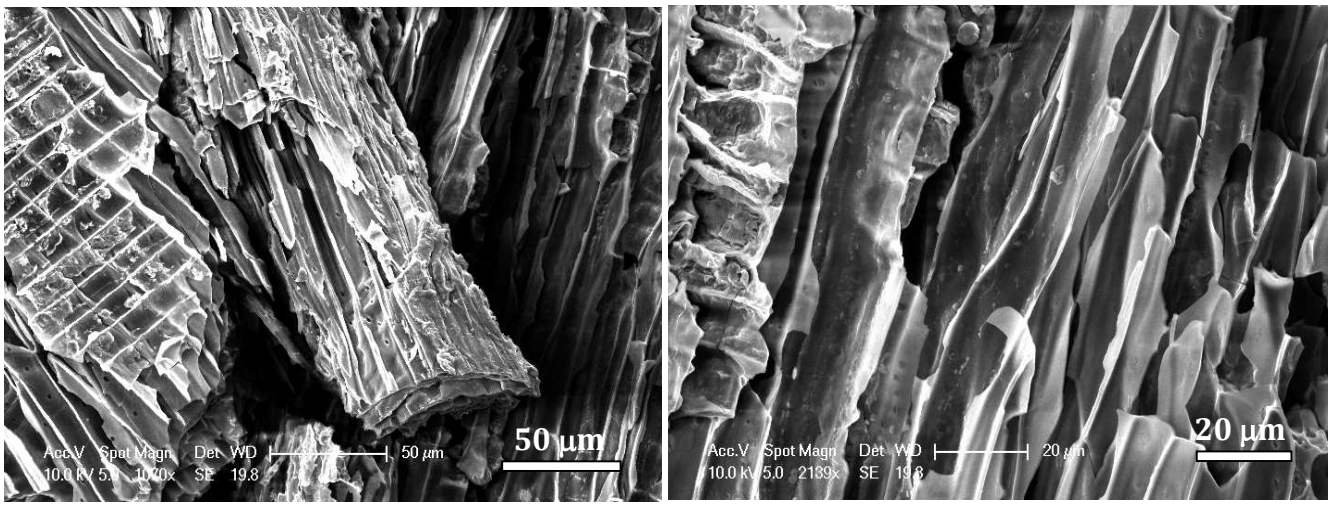

Figure 2. SEM images of ACSD carbon generated via flash carbonization of sawdust at 400 °C.

3.2 Yield and properties of activated ACSD carbons

We monitored the activated carbon yield from the flash carbonisation route in comparison to conventional synthesis routes. We first note that for conventional activation (i.e., via hydrothermal carbonisation (HTC) of the sawdust to hydrochar followed by activation of the hydrochar), the yields are as follows; the hydrochar yield from sawdust is ca. 40%,[22,42,43] while the yield of activated carbons from the hydrochar (and other activateable carbon sources) varies between 15 and 50%.[14,22,44-46] This means that the yield of activated carbon with respect to the starting sawdust ranges from ca. 4% to 20%. On the other hand, the flash carbonisation of sawdust to ACSD carbon resulted in carbon yield of between 31% and 40%, while the yield of activated carbon from the ACSD carbon (at KOH/carbon ratio of 2) was typically between 50% (at 800 °C) and 60% (at 600 °C). Therefore, for the flash carbonization route, the yield of activated carbon with respect to the raw sawdust was between 15 and 24%, which is comparable if slightly better than that of the more conventional HTC route. This comparison clarifies that the flash carbonisation route does not present any disadvantages with respect to activated carbon yields; the yields are comparable to what is generally observed for activated carbons with moderate to high porosity. [14,22,44-46] It is also noteworthy that the yields of activated carbon from the ACSD carbon observed here (50 to 60%)

are higher than normal (10 to 40%), and are comparable to those reported for activation of CNL1 carbon (30 – 80 wt%).[40] This is not unexpected given that the CNL1 carbon was generated via a process akin to flash carbonization.

The TGA curves of the activated ACSD-xT carbons following heating under flowing air conditions are shown on Figure 1. The activated carbons exhibit higher thermal stability compared to the ACSD carbon and the stability increases with rise in activation temperature or extent of activation (cf. sample ACSD-2800 vs ACSD-4800). Similar to the ACSD carbon, the activated carbons are completely burnt off with no residual mass (Figure 1). The burn off occurs in one step between 320 and 600 ^{o}C, and the temperature at which maximum burn-off ensues rises from 420 ^{o}C for ACSD carbon to 490 ^{o}C (ACSD-2600), 515 ^{o}C (ACSD-2700), 540 ^{o}C (ACSD-2800) and 560 ^{o}C (ACSD-4800). The trend is similar to what has previously been observed for KOH activated carbons such as activated CNLI carbon[40] and activated carbons derived from poplar anthers wherein the temperature of maximum combustion increased from 500 to 590 ^{o}C as activation temperature rose from 500 to 800 ^{o}C.[31] Elemental composition data (CHNO analysis) of the activated samples is given in Table 1. On activation of the ACSD carbon, the elemental carbon content rises from 72.4 wt% to between 78 and 90 wt% depending on the level of activation. On the other hand, the H content reduces from 3.2 wt% to between 1.9 and 0.4 wt%, with lower content at the higher levels of activation (i.e., samples ACSD-2800 and ACSD-4800). The amount of O also reduces gradually as the level of activation increases from 24 wt% (for ACSD carbon) to as low as 11 wt% for sample ACSD-4800.

The XRD patterns of the ACSD-xT activated carbons (Figure S4) show weak features centred on $2\theta = 22^{o}$ and 44^{o}, which are, respectively, very weak diffractions of (002) and (100) planes of disordered graphitic domains. The XRD patterns of carbons activated at higher temperature (ACSD-2800 and ACSD-4800) show a clearer (100) diffraction (at $2\theta \sim 44^{o}$). This may be an indication of a higher level of graphitization and is consistent with the greater thermal

stability of these carbons according to TGA data (Figure 1). Raman spectra for the activated carbons are shown in Figure 2, and exhibit bands at 1335 - 1350 cm^{-1} and 1580 - 1590 cm^{-1}, which are the D-peak (disordered carbon) and the G-peak (graphitic domains), respectively.[47] The ratio of peak intensity between the D-peak and G-peak (i.e., the I_D/I_G ratio) was calculated using the two-band fitting model. The I_D/I_G ratio (Supporting Table S2) is 0.86 (ACSD-2600) and gradually increases for higher activation levels to 0.91 (ACSD-2700), 0.93 (ACSD-2800) and 0.94 (ACSD-4800). The increase suggests that greater activation acts to disrupt the ordering of graphitic domains. It is noteworthy that at any given level of activation, the I_D/I_G ratio of the flash carbonization derived carbons is generally greater than that of hydrothermal carbonization derived carbons (Table S2). Regarding the overall level of graphitization, the I_D/I_G ratios of between 0.86 and 0.94 are consistent with the predominantly amorphous nature of the carbons.[47]

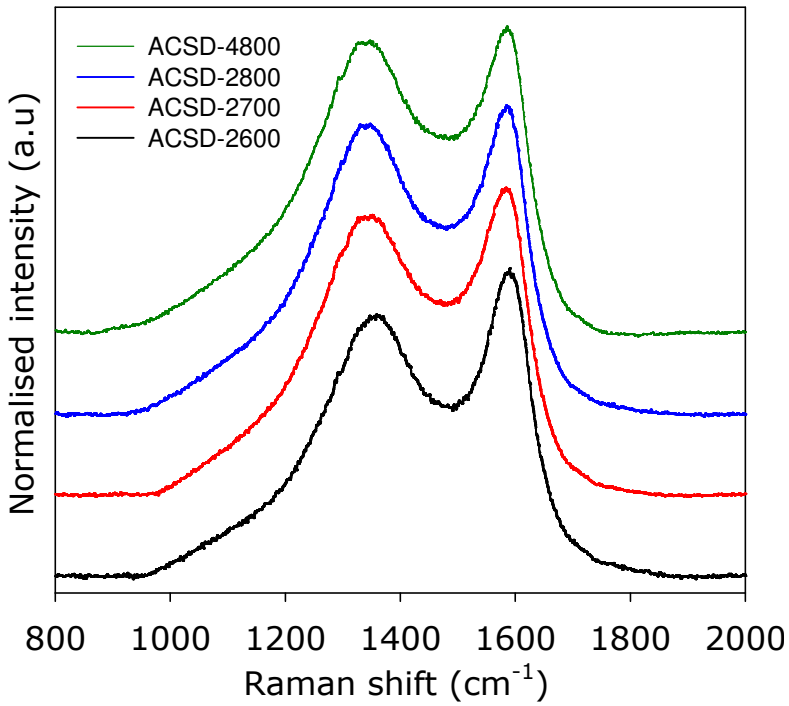

Figure 2. Raman spectra of sawdust-derived flash carbonized activated ACSD-xT carbons. See experimental section for sample designation.

The nitrogen sorption isotherms obtained for the activated ACSD-xT carbons are shown in Figure 3A. The isotherms of all the carbons are type I, which is normally associated with materials whose porosity is dominated by micropores.[48] The amount of nitrogen adsorbed increases with the severity of activation (i.e., at higher activation temperature and/or KOH/carbon ratio). However, for the carbons activated at KOH/carbon ratio of 2, the activation temperature 600, 700 or 800 ºC) does not appear to have any effect on the nature and shape of the isotherm; all the isotherms of ACSD-2T carbons exhibit a sharp adsorption knee, which is consistent with the presence of a high proportion of microporosity. This observation contrasts with most previous reports wherein a rise in activation temperature results in isotherms with a gradual widening of the adsorption knee,[44,46,49-57] but is akin to the behaviour of recently described activated carbons derived from burnt wood that was generated in a process similar to the flash carbonisation used in the present study.[40] It is noteworthy that even the most severely activated carbon (ACSD-4800) still exhibits an isotherm indicative of significant microporosity. As shown in Figure 3B, all the carbons possess pore channels of size < 15 Å, and typically below 10 Å, especially for ACSD-2T samples. The main pore size maxima values derived from Figure 3B are given in Table 2. Sample ACSD-2600 and ACSD-2700 are dominated by 8.5 Å pores, while for sample ACSD-2800 the pores are slightly larger at 9.0 Å, thereby showing a very slight increase in pore size at higher activation temperature. As expected, sample ACSD-4800 has larger pores and a wider pore size distribution but, remarkably for such severe activation conditions, still within the micropore range (i.e., hardly any pores larger than 20 Å are observed).

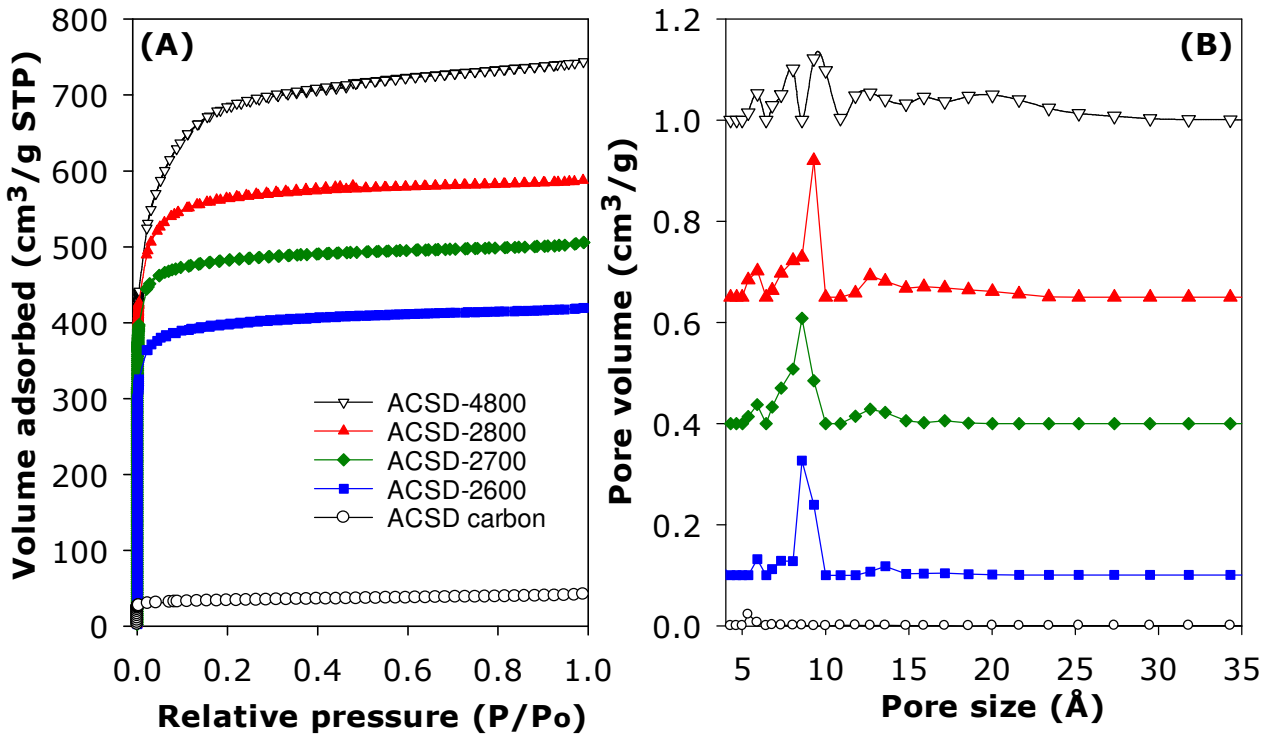

Figure 3. (A) Nitrogen sorption isotherms and (B) pore size distribution curves of flash carbonized activated ACSD-xT carbons. Data for the raw ACSD carbon is included for comparison. Y-axis in (B) shows incremental pore volume.

Table 2. Textural properties and CO_2 uptake of ACSD-xT activated carbons derived from air-carbonized sawdust.

Sample	Surface area[a] (m^2 g^{-1})	Pore volume[b] (cm^3 g^{-1})	Pore size[c] (Å)	CO_2 uptake[d] (mmol g^{-1})		
				0.15 bar	1 bar	20 bar
ACSD-2600	1511 (1338)	0.65 (0.54)	8.5	1.2	4.3	12.0
ACSD-2700	1830 (1657)	0.78 (0.67)	8.5/13	1.1	4.9	14.0
ACSD-2800	2163 (1866)	0.93 (0.74)	9/13	1.1	4.7	16.8
ACSD-4800	2610 (1892)	1.15 (0.74)	6/8/10/16	0.9	4.0	19.7

The values in the parenthesis refer to: [a]micropore surface area and [b]micropore volume. [c]Pore size distribution maxima obtained from NLDFT analysis. [d]CO_2 uptake at 25 °C and various pressures (i.e., 0.15 bar, 1 bar and 20 bar).

The textural properties of the ACSD-xT carbons are summarized in Table 2. The surface area is, in the context of activated carbons, moderate to high depending on the severity of activation. A gradual increase in surface area is noted from 1511 $m^2 g^{-1}$ for ACSD-2600 to 2163 $m^2 g^{-1}$ for ACSD-2800. As expected, the most severely activated carbon (ACSD-4800) has the highest surface area of 2610 $m^2 g^{-1}$. The total pore volume follows a similar trend and is in the range 0.65 – 0.93 $cm^3 g^{-1}$ for ACSD-2T carbons and 1.15 $cm^3 g^{-1}$ for sample ACSD-4800. The high microporosity of the present samples is manifested by the proportion of surface area and pore volume arising from micropores, which for ACSD-2T samples is typically ca. 90% for surface area and 80 - 85 % for pore volume, while for the most severely activated sample (ACSD-4800) it is still remarkably high at ca. 70% (surface area) and 65% (pore volume). We compared the textural properties of the flash carbonized samples to carbons (designated as SDxT) prepared from sawdust via a more conventional hydrothermal carbonization (HTC) route (Supporting Table S3). At any given level of activation (i.e., similar temperature and KOH/carbon ratio), the flash carbonized ACSD-2T carbons have comparable surface area and pore volume to analogous SD2T samples. However, ACSD-2T samples have a higher proportion of microporosity especially for activation at 800 ^oC (sample ACSD-2800 vs SD2800). For activation at KOH/carbon ration of 4 and 800 ^oC, although the samples have comparable total surface area (Table S3), the flash carbonized ACSD-4800 sample has significantly lower pore volume and much greater proportion of microporosity compared to the HTC SD4800 sample (Supporting Figure S5). This apparent resistance to formation of large pores indicates that the flash carbonized ACSD carbon is somewhat resistant to activation in a manner similar to that of the recently reported air carbonized CNL1 carbon.[40] This is not unexpected as both these raw carbons are generated via carbonization in the presence of air. Indeed a comparison of the textural properties of ACSD-xT samples with those of activated CNL1 carbons (Supporting Table S4) shows that both sets of samples have consistently high

levels of microporosity even at severe levels of activation (sample ACSD-4800 and CNL1-4800).

The data discussed above indicates that flash carbonization is a viable route for the preparation of activated carbons, whilst offering some advantages in terms of simplicity, ease of preparation and reduction of energy costs resulting from the low carbonization temperature (400 ºC vs typically > 800 ºC) and/or quick carbonization process (<10 minutes vs typically > 1 h for air-free carbonization or hydrothermal carbonisation). However, it is also necessary to more clearly place the nature of the flash carbonized samples in a proper context (i.e., when compared to other routes and precursors to activated carbons), and also to ascertain the reproducibility of the flash carbonization process. We therefore compared the textural properties of the activated ACSD-xT carbons with a range of similarly activated (i.e., at 800 ºC and KOH/carbon ratio of 2 or 4) carbons derived from lignin[12] or grass[13] via hydrothermal carbonization or directly from so-called air-carbonised CNL1 carbon,[40] carbon nanotube superstructures[50] or polypyrrole.[46] It is clear from the comparison (Table S5) that ACSD-xT carbons possess levels of microporosity that are closest to those of activated CNL1 carbons, and in any case far higher than for the other sets of carbons. The tendency to generate micropores rather than larger pores may be explained by considering that performing flash carbonization in the presence of air can act to enrich the proportion of lignin products (relative to other woody components such as cellulose) as the later are more readily oxidized (i.e. burnt) in air.[58-64] Such lignin enriched carbonaceous matter is known to be less susceptible to activation in a manner similar to that observed here for the ACSD carbon.[62-64] Regarding reproducibility of the flash carbonization route, we compared textural data from two separate preparations (at 700 or 800 ºC and KOH/carbon ratio of 2) performed several months apart and with each synthesis stating from the raw sawdust. The nitrogen sorption isotherms and pore size distribution curves of samples from the two preparations are virtually identical (Supporting

Figure S6). Furthermore, the samples have remarkably good agreement with respect to their textural properties (Supporting Table S6), which offers ample evidence of the reproducibility of the present flash carbonization route for the synthesis of activated carbons.

As shown by the SEM images in Figure 2 above, the particle morphology of the ACSD carbon is comprised of extended honeycomb structures that have the appearance of being retained from the woody structure of the sawdust starting material. On activation, the particle morphology undergoes significant change although some honeycomb-like structures are still partly retained as shown in Figure 4 (and supporting Figures 7 and 8). The morphology of the activated carbons is mainly made up of particles with relatively smooth surfaces characterized by large conchoidal cavities, which is similar to what has previously been reported for carbons generated via the hydrothermal carbonization route.[14] A closer examination of the SEM images of the ACSD carbon before (Figure 2) and after (Figure 4, S7 and S8) activation reveals that woody particle morphology is retained in a manner that is unlike what is observed for samples derived from hydrochar.[14] The present carbons possess larger aggregates of interlinked monolith-like particles. This apparent particle connectivity may be ascribed to two factors; (i) preservation of woody morphology during the flash carbonization (as opposed to HTC wherein the particle morphology completely changes to spherical structures[14]), and (ii) low levels of particle disruption during the activation process due to the resistant (to activation) nature of the ACSD carbon. The TEM images in Figure 5 confirm the presence of disordered pore channels, which is typical for activated carbons. It is possible to observe that the size of the pore channels for sample ACSD-4800 is larger than for the ACSD-2T samples, which is consistent with the porosity data discussed above.

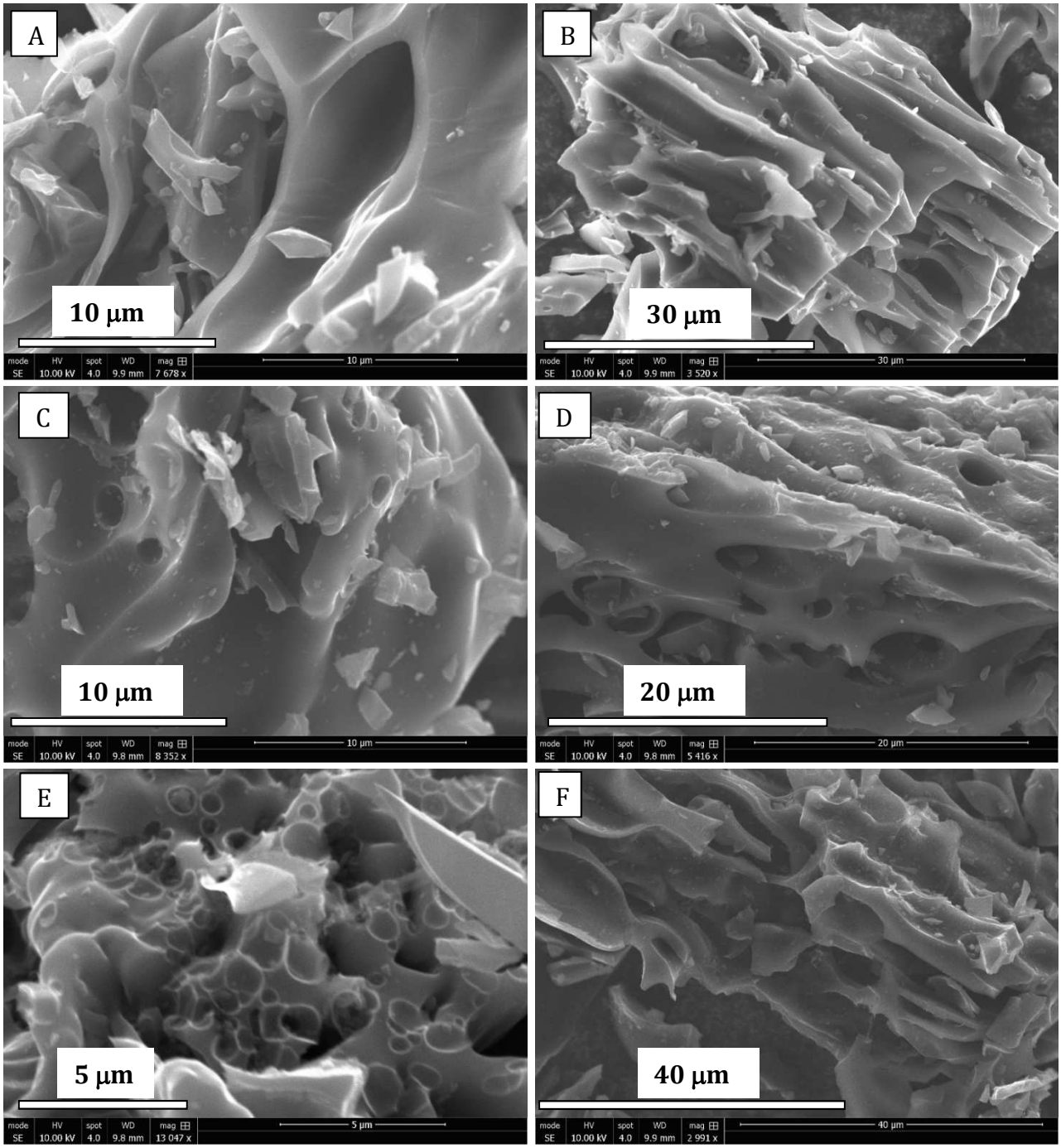

Figure 4. SEM images of sawdust-derived flash carbonized activated ACSD-2T carbons prepared at KOH/carbon ratio of 2 at temperature (T) of 600, 700 or 800 ^{o}C; ACSD-2600 (A, B), ACSD-2700 (C, D) and ACSD-2800 (E, F).

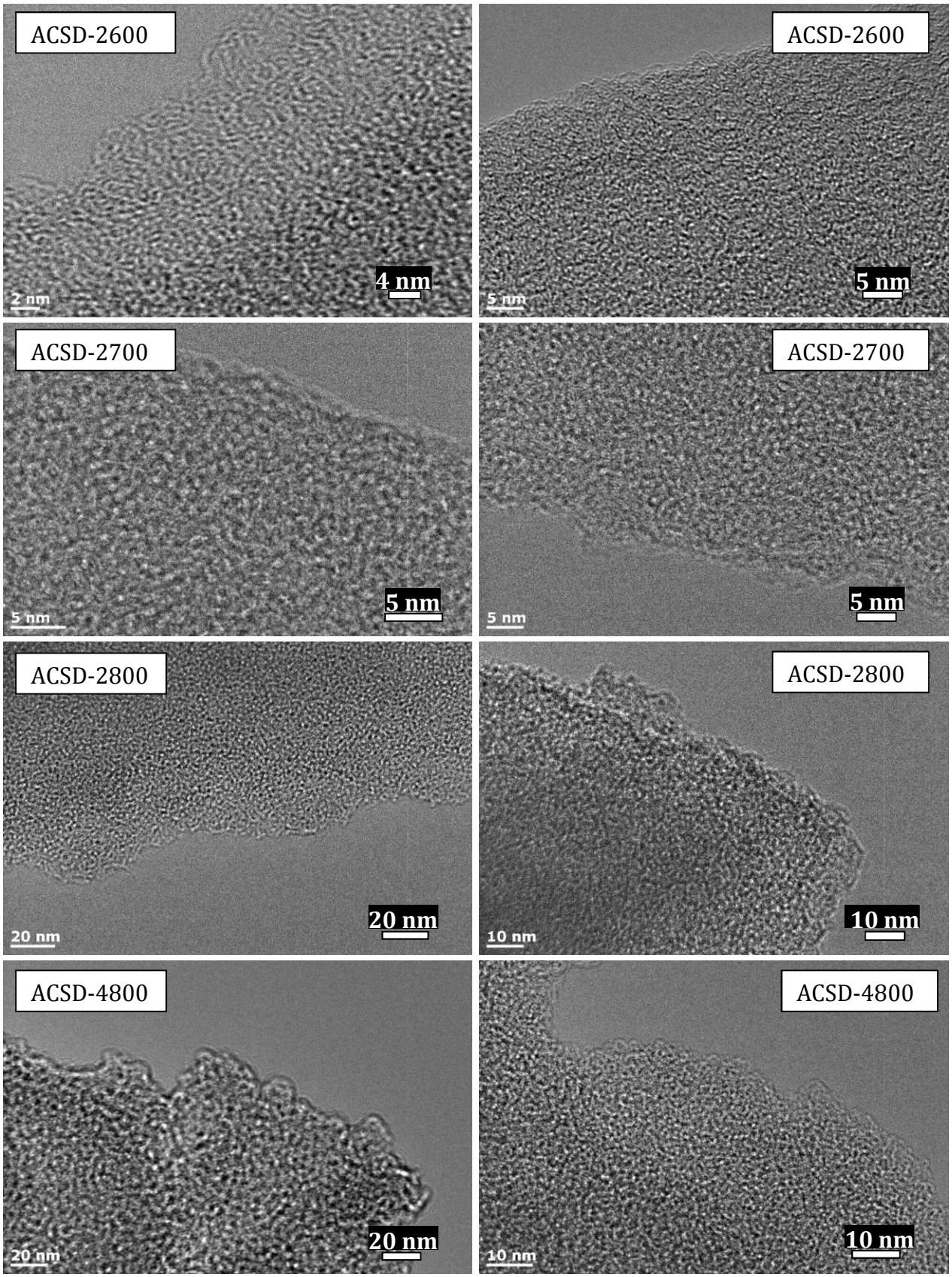

Figure 5. TEM images of sawdust-derived flash carbonized activated ACSD-*x*T carbons, where *x* is the KOH/carbon ratio (2 or 4) and T is activation temperature (600, 700 or 800 ^{o}C).

3.3 CO_2 uptake capacity of activated ACSD carbons

3.3.1 Gravimetric storage capacity

Activated carbons are currently considered to be one of the most attractive classes of materials for application in CO_2 capture and storage both for pre and post-combustion scenarios. Indeed, in recent years, carbons generated from a variety of sources (including biomass) have shown significant promise for CO_2 storage under conditions that mimic post-combustion scenarios. The present carbons offer some advantages in terms of simplicity of their synthesis over activated carbons prepared via longer routes that include either hydrothermal carbonisation or high temperature pyrolysis and would thus be attractive as CO_2 storage materials. We therefore determined the CO_2 storage capacity of the ACSD-xT carbons at room temperature (25 ^oC) and low to medium pressure (0 to 20 bar), and the uptake isotherms are shown in Figure 6 (and supporting Figure S9) while the storage capacity at various key pressures (0.15, 1 and 20 bar) is summarised in Table 2. At a pressure of 1 bar (Figure 6 and S9), the carbons store between 4.0 and 4.9 mmol g^{-1} of CO_2, which is at the top end of what has been observed for all porous carbonaceous materials.[12-16,38-40,49-57,65-72] The uptake is greatest for the samples (ACSD-2700 and ACSD-2800) with the highest proportion of microporosity *and* few or no pores greater than 10 Å. The carbons also have attractive uptake at very low pressure (0.15 bar) of between 0.9 and 1.2 mmol g^{-1}. At 20 bar, the uptake is determined by the total surface area and thus sample ACSD-4800 performs best with storage capacity of close to 20 mmol g^{-1}. The storage capacity of ACSD-4800 is interesting in that the sample shows very attractive performance *both* at low pressure (post-combustion) and high pressure (pre-combustion) conditions.

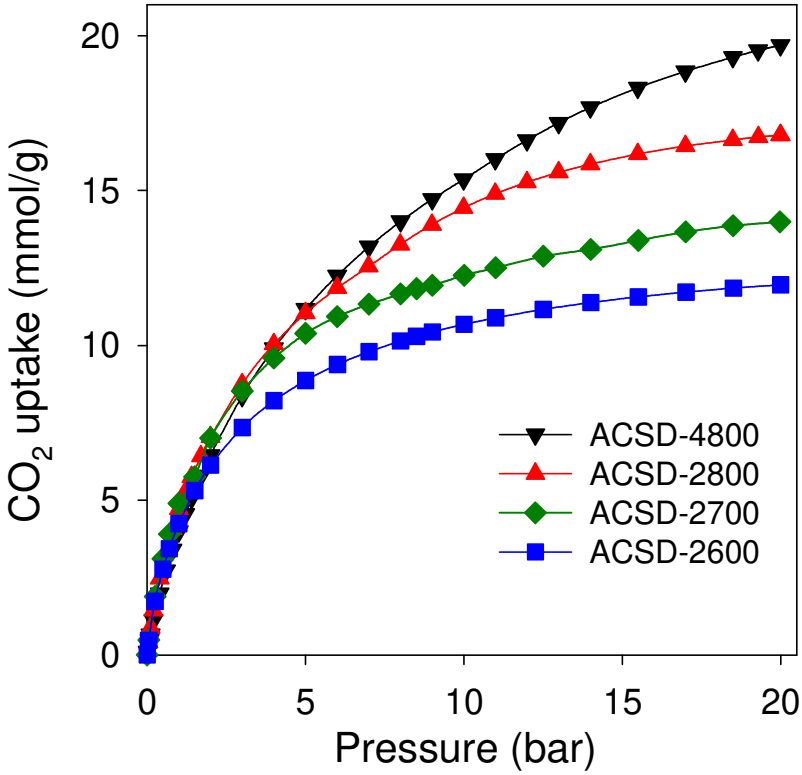

Figure 6. CO_2 uptake isotherms at 25 ^oC and 0 - 20 bar for sawdust-derived flash carbonized activated ACSD-xT carbons. See experimental section for sample designation.

The CO_2 storage capacity of the present flash carbonised carbons matches or outperforms that of analogous samples prepared via more conventional hydrothermal carbonisation (Supporting Table S3 and supporting Figure S10 and S11). This is particularly the case at pressure of 0.15 and 1 bar for carbons prepared at 800 ^oC. At 0.15 bar (i.e., conditions that closely mimic post-combustion flue gas streams from power stations that tend to consist of ca. 15% CO_2, 70–75% N_2 and 5–7% water) the CO_2 uptake of ACSD-x800 flash carbonised samples is 40 - 50% higher than for analogous SDx800 HTC samples, while at 1 bar it is greater by ca. 35% (Table S3). At 20 bar, the CO_2 uptake of the ACSD carbons is higher or comparable to that of HTC samples. The greater uptake of the ACSD samples at low pressure (0.15 and 1 bar) may be ascribed to their higher levels (i.e., proportion) of microporosity. However, it is interesting to note that the ACSD carbons also outperform so-called activated CNL1 carbons that also possess high levels of microporosity (Table

S4). The general picture that emerges is that the flash carbonised samples, despite being prepared via a simpler, and potentially cheaper and more direct route, offer very attractive CO_2 uptake that is amongst the highest reported so far for porous carbons. [12-16,38-40,49-57,65-72]

3.3.2 Working capacity for pressure-swing adsorption (PSA) and vacuum-swing adsorption (VSA)

Currently, most operations that require large-scale post-combustion capture and storage of CO_2 from flue gas streams rely on so-called amine scrubbing processes that chemically bind the CO_2. One of the main challenges encountered in the amine scrubbing process is that significant thermal treatment is required in order to overcome the strong binding between the CO_2 molecules and amines during the desorption/recycling step. The thermal treatment necessitates temperature swing adsorption (TSA) processes that take up large amounts of energy thus making the process energy inefficient.[73,74] For this reason, much recent research has been aimed at exploring alternative energy efficient processes that can achieve the removal of CO_2 from flue gas streams. Such processes may rely on sorption (adsorption and desorption) of CO_2 on solid state adsorbents via either pressure swing adsorption (PSA) or vacuum swing adsorption (VSA).[75,76] We therefore explored the performance of the ACSD-xT carbons for such processes. Our data simulates a number of scenarios, namely; (i) a PSA system wherein adsorption of CO_2 takes place at a pressure of 6 bar followed by desorption (i.e., recycling) at 1 bar, (ii) a VSA system with adsorption a pressure of 1.5 bar and recycling at ca. 0.05 bar.[77] This was done for a pure CO_2 stream with the aforementioned pressure values and a 20% CO_2 stream for which the pressure values are appropriately scaled down to 1.2 bar (adsorption) to 0.2 bar (desorption) for PSA; and 0.3 bar (adsorption) to 0.01 bar (desorption) for VSA. The working capacity for the PSA and VSA processes is presented in Table 3. For a pure CO_2 stream, the PSA working capacity for all the ACSD-xT samples is very attractive at between 5.2 and 8.3 mmol g^{-1}. To put these working capacity values in context, we note that at the top

end (8.3 mmol g^{-1}) they are higher than those of the best performing materials to date, such as metal organic frameworks (MOFs) with open-metal sites (3.5 mmol g^{-1} for Mg-MOF-74 and 7.8 mmol g^{-1} for HKUST-1),[78] and far exceed the performance (1.6 mmol g^{-1}) zeolite NaX[79], as shown in Table 3. Furthermore, when compared to the current state-of-the-art carbons (Supporting Table S7), the PSA working capacity of the ACSD-xT carbons also exceeds those derived from air-carbonised carbonaceous matter (6.3 mmol g^{-1} for CNL1-2800),[40] organic metal salts (4.3 mmol g^{-1} for CKHP800-1-C5)[52] or from sawdust hydrochar (7.9 mmol g^{-1} for SD4800).

Table 3. Gravimetric working capacity for pressure swing adsorption (PSA) and vacuum swing adsorption (VSA) of CO_2 on activated ACSD-xT carbons, and benchmark porous materials at 25 ºC for a pure CO_2 gas stream and a 20% partial CO_2 pressure flue gas.

Sample	Pure CO_2 uptake[a] (mmol g^{-1})		Flue gas CO_2 uptake[b] (mmol g^{-1})	
	PSA	VSA	PSA	VSA
ACSD-2600	5.2	4.8	3.4	2.0
ACSD-2700	6.1	5.3	3.7	2.1
ACSD-2800	7.5	5.6	3.8	1.7
ACSD-4800	8.3	5.0	5.3	1.5
HKUST-1[c]	7.8	6.4	4.5	1.6
Mg-MOF-74[c]	3.5	3.9	2.1	4.1
NaX[d]	1.6	2.8	1.8	2.5

[a]1 bar to 6 bar for PSA; 0.05 bar to 1.5 bar for VSA. [b]0.2 bar to 1.2 bar for PSA; 0.01 bar to 0.3 bar for VSA. [c]Data from reference 78. [d]Data from reference 79.

Under simulated flue gas conditions that mimic post-combustion CO_2 capture, the PSA working capacity of the ACSD-xT carbons is between 3.4 and 5.3 mmol g^{-1}, which is higher than that of benchmark carbons (Table S7) and also, importantly, as shown in Table 3 exceeds

the performance of Mg-MOF-74 (2.1 mmol g^{-1}), HKUST-1 (4.5 mmol g^{-1}), and zeolite NaX (1.8 mmol g^{-1}).[78,79] The working capacity for VSA uptake is also attractive, being in the range of 4.8 to 5.6 mmol g^{-1} (for pure CO_2 stream) and 1.5 to 2.1 mmol g^{-1} (under simulated flue gas conditions). These values are higher than those of benchmark carbons (Table S7), and are comparable to the performance of Mg-MOF-74 and HKUST-1.[78]

Although the gravimetric CO_2 working capacity of the ACSD-xT carbons is impressive, it is also important to consider the volumetric storage capacity. This is particularly relevant for post-combustion capture from flue gas streams wherein the carbons would be packed into a column with defined space, which means that the amount of CO_2 stored by the adsorbent per given space (i.e., volume) in the column is a key factor. The volumetric working capacity can be determined if the packing density of the carbons is known. The packing density of porous carbons can be estimated from their experimentally determined skeletal density according to the equation: packing density = $(1/\rho_s+V_T)^{-1}$, where ρ_s is the skeletal density and V_T is the total pore volume. Using helium sorption at 0 ^oC,[80] we determined the skeletal density of the ACSD-xT carbons to be 2.1–2.2 g cm^{-3}, and accordingly estimated their packing density (in g cm^{-3}) to be 0.90 (ACSD-2600), 0.81 (ACSD-2700), 0.73 (ACSD-2800) and 0.62 for ACSD-4800. These packing density values are comparable to those of previously reported lowly activated carbons.[81] The volumetric working capacity of the activated ACSD-xT carbons (Table S8) outperforms that of benchmark MOF and zeolite NaX materials due to the combination of both a higher gravimetric capacity and high packing density. For a pure CO_2 stream the ACSD-xT samples have a PSA volumetric working capacity of between 208 and 280 g l^{-1} (i.e., 4.7 – 6.3 mmol cm^{-3}), which is much higher than that of HKUST-1 (147 g l^{-1} or 3. 3 mmol cm^{-3}), Mg-MOF-74 (63 g l^{-1} or 1.43 mmol cm^{-3}) and zeolite NaX (44 g l^{-1} or 1 mmol cm^{-3}). Equally attractive is the Pure CO_2 stream VSA volumetric working capacity of 136 – 190 g l^{-1} (i.e., 3.1 – 4.3 mmol cm^{-3}) compared to 121 g l^{-1} (2.8 mmol cm^{-3}), 70 g l^{-1} (1.6 mmol cm^{-3}) and 78 g l^{-1}

(1.8 mmol cm^{-3}) for HKUST-1, Mg-MOF-74 and zeolite NaX, respectively. More importantly, for simulated flue gas conditions, the PSA volumetric working capacity of the ACSD-xT carbons is in the range of 122 to 145 g l^{-1} (2.8 – 3.3 mmol cm^{-3}), which outperforms that of zeolite NaX (50 g l^{-1}; 1.1 mmol cm^{-3}), HKUST-1 (85 g l^{-1}; 1.9 mmol cm^{-3}) and Mg-MOF-74 (38 g l^{-1}; 0.86 mmol cm^{-3}). The associated VSA volumetric working capacity of 52 – 87 g l^{-1} (1.2 – 2.0 mmol cm^{-3}), is superior to the 74 g l^{-1} (1.7 mmol cm^{-3}), 30 g l^{-1} (0.7 mmol cm^{-3}) and 69 g l^{-1} (1.6 mmol cm^{-3}) achieved by Mg-MOF-74, HKUST-1 and zeolite NaX, respectively (Table S8). The performance of the ACSD-xT carbons is comparable to that of activated carbons derived from air-carbonised CNLI carbons (Table S8). A key difference is that the present ACSD-xT samples were deliberately and reproducibly prepared.

4. Conclusions

Biomass derived activated carbons were successfully produced via a flash carbonization route that offers simplicity by removing the need for extended hydrothermal carbonisation or pyrolysis. The flash carbonization route involved the brief (< 10 minutes) carbonization of sawdust in air at a low temperature (400 ^{o}C) prior to activation. The flash carbonisation of sawdust generates carbonaceous matter that is resistant to activation (with KOH) and consequently results in activated carbons that retain a high proportion of microporosity even after undergoing severe activation. The porosity of the flash carbonized activated carbons is dominated by pore channels of size 8 – 9 Å, which offer excellent post-combustion CO_2 uptake of up to 5 mmol g^{-1} at 1 bar and 25 ^{o}C. Interestingly, depending on the level of activation, it is possible to tailor the porosity towards carbons with simultaneously high post (< 1 bar) and pre (20 bar) combustion CO_2 capture. The carbons also exhibit very attractive working capacity for CO_2 capture for low pressure swing operations, i.e., 5.2 – 8.3 mmol g^{-1} for pressure swing adsorption (PSA) for a simulated pure CO_2 stream (6 to 1 bar) and 3.4 – 5.3 mmol g^{-1} for a

simulated flue gas stream (1.2 to 0.2 bar). For vacuum swing adsorption (VSA), the carbons also have attractive working capacity of 4.8 – 5.6 mmol g^{-1} for pure CO_2 (1.5 to 0.05 bar), and 1.5 – 2.1 mmol g^{-1}) for flue gas (0.3 to 0.01 bar). These high gravimetric working capacity values translate to very attractive volumetric capacity. Overall, the CO_2 uptake performance of the flash carbonised carbons is comparable or better than that of current benchmark porous materials including carbons, zeolites or metal organic frameworks.

Supporting Information

Eight tables with comparative data on elemental composition, porosity and CO_2 uptake. Eleven additional figures; XRD patterns, SEM images, comparative nitrogen sorption and pore size distribution curves, comparative trends in porosity of activated ACSD carbons, and comparative low to high pressure gravimetric CO_2 uptake isotherms.

Acknowledgements

We are thankful to the Nanoscale and Microscale Research Centre (nmRC) at the University of Nottingham for assistance with SEM and TEM analysis, and Raman spectra.

References

1. L. Schlapbach and A. Züttel, *Nature* 2001, **414**, 353.
2. M. Sevilla and R. Mokaya, *Energy Environ. Sci*., 2014, **7**, 1250.
3. L. Wei and G. Yushin, *Nano Energy,* 2012, **1,** 552.
4. J. C. Wang and S. Kaskel, *J. Mater. Chem*., 2012, **22**, 23710.
5. J. A. Turner, *Science* 1999*,* **285**, 687.
6. Y. X. Xia, Z. X. Yang and Y. Zhu, *J. Mater. Chem. A,* 2013, **1** 9365.
7. J. Ji, L. L. Zhang, H. Ji, Y. Li, X. Zhao, X. Bai, X. Fan, F. Zhang and R. S. Ruoff, *ACS Nano*, 2013, **7**, 6237.

8. Y. Zhu, S. Murali, M. D. Stoller, K. J. Ganesh, W. Cai, P. J. Ferreira, A. Pirkle, R. M. Wallace, K. A. Cychosz, M. Thommes, D. Su, E. A. Stach and R. S. Ruoff, *Science*, 2011, **332**, 1537.
9. C. Liu, F. Li, L-P. Ma and H-M. Cheng, *Adv. Mater*. 2010, **22**, E28–E62.
10. M. Sevilla and A. B. Fuertes, *Energy Environ. Sci.,* 2011, **4**, 1765.
11. M. M. Titirici, R. J. White, C. Falco and M. Sevilla, *Energy Environ. Sci*. 2012, **5,** 6796.
12. W. Sangchoom and R. Mokaya, *ACS Sust. Chem. Eng*., 2015, **3**, 1658.
13. H. M. Coromina, D. A. Walsh and R. Mokaya, *J. Mater. Chem. A* 2016, **4**, 280.
14. M. Sevilla, A. B. Fuertes and R. Mokaya, *Energy Environ. Sci*., 2011, **3**, 1400.
15. C. Robertson and R. Mokaya, *Micropor. Mesopor. Mater.,* 2013, **179**, 151.
16. N. Balahmar, A. C. Mitchell, and R. Mokaya, *Adv. Energy Mater.*, **2015**, *5*, 1500867
17. L. Wei, M. Sevilla, A. B. Fuertes, R. Mokaya and G. Yushin, *Adv. Energy Mater*., 2011, **1**, 356.
18. M. Sevilla, W. Sangchoom, N. Balahmar, A. B. Fuertes and R. Mokaya, *ACS Sust. Chem. Eng*., 2016, **4**, 4710.
19. J. A. Libra, K. S. Ro, C. Kammann, A. Funke, N. D. Berge, Y. Neubauer, M. M. Titirici, C. Fühner, O. Bens, J. Kern and K. H. Emmerich, *Biofuels*, 2011, **2**, 89.
20. M. M. Titirici and M. Antonietti, *Chem. Soc. Rev*., 2010, **39**, 103.
21. B. Hu, K. Wang, L. Wu, S. H. Yu, M. Antonietti and M. M. Titirici, *Adv. Mater*., 2010, **22**, 813.
22. M. Sevilla and A. B. Fuertes, *Carbon*, 2009, **47**, 2281.
23. A. Demirbas and G. Arin, *Energy Sources*, 2002, **24**, 471.
24. F. Shafizadeh, *J. Anal. Appl. Pyrolysis*, 1982, **3**, 283.
25. A.V. Bridgwater, D. Meier and D. Radlein, *Org. Geochem*., 1999, **30**, 1479.
26. M. X. Fang, D. K. Shen, Y. X. Li, C. J. Yu, Z. Y. Luo, K. F. Cen, *J. Anal. Appl. Pyrolysis*, 2006, **77**, 22.
27. M. Molina-Sabio and F. Rodriguez-Reinoso, *Colloids Surf., A,* 2004, **241**, 15.
28. F. Wu, R. Tseng and R. Juang, *Sep. Purif. Technol.*, 2005, **47**, 10.
29. F. Wu and R. Tseng, *J. Colloid Interface Sci.*, 2006, **294**, 21.
30. K. Yang, J. Peng, C. Srinivasakannan, L. Zhang, H. Xia and X. Duan, *Bioresource Technol.*, 2010, **101**, 6163.
31. J. Song, W. Shen, J. Wang and W. Fan, *Carbon,* 2014, **69**, 255.
32. Z. Hu, M.P. Srinivasan and Y. Ni, *Carbon,* 2001, **39**, 877.
33. F. Caturla, M. Molina-Sabio and F. Rodríguez-Reinoso, *Carbon,* 1991, **29**, 999.

34. M. Jagtoyen and F. Derbyshire, *Carbon*, 1998, **7**, 1085.
35. M. C. Baquero, L. Giraldo, J. C. Moreno, F. Suárez-García, A. Martínez-Alonso and J. M. D. Tascón, *J. Anal. Appl. Pyrolysis*, 2003, **70**, 779.
36. W. Xing, C. Liu, Z. Zhou, L. Zhang, J. Zhou, S. Zhuo, Z. Yan, H. Gao, G. Wang and S. Z. Qiao, *Energy Environ. Sci.*, 2012, **5**, 7323.
37. M. Sevilla and R. Mokaya, *J. Mater. Chem.* 2013, **21**, 4727.
38. N. P. Wickramaratne and M. Jaroniec, *J. Mater. Chem. A.,* 2013, **1**, 112.
39. B. Adeniran and R. Mokaya, *Chem. Mater.* 2016, **28**, 994.
40. E. Haffner-Staton, N. Balahmar and R. Mokaya, *J. Mater. Chem. A* 2016, **4**, 13324.
41. K. Y. Foo and B. H. Hameed, *Bioresour. Technol.*, 2012, **111**, 425.
42. E. Sermyagina, J. Saari, J. Kaikko and E. Vakkilainen, *J. Anal. Appl. Pyrolysis*, 2015, **113**, 551.
43. Z. Liu, A. Quek, S. K. Hoekman, R. Balasubramanian, *Fuel*, 2013, **103**, 943.
44. M. Sevilla, A. B. Fuertes and R. Mokaya, *Int. J. Hydrogen Energy,* 2011, **36**, 15658.
45. B. Adeniran and R. Mokaya, *Nano Energy*, 2015, **16***,* 173.
46. M. Sevilla, R. Mokaya and A. B. Fuertes, *Energy Environ. Sci.*, 2011, **4**, 2930.
47. A. C. Ferrari and J. Robertson, *Phys. Rev. B*, 2000, **61**, 14095.
48. K. S. W. Sing, D. H. Everett, R. A. W. Haul, L. Moscou, R. A. Pierotti, J. Rouquerol and T. Siemieniewska, *Pure Appl. Chem*., 1985, **57**, 603.
49. N. P. Wickramaratne and M. Jaroniec, *ACS Appl. Mater. Interfaces*, 2013, **5**, 1849.
50. B. Adeniran and R. Mokaya, *J. Mater. Chem. A*, 2015, **3**, 5148.
51. Z. Zhang, J. Zhou, W. Xing, Q. Xue, Z. Yan, S. Zhuo and S. Z. Qiao, *Phys. Chem. Chem. Phys.,* 2013, **15**, 2523.
52. B. Adeniran, E. Masika and R. Mokaya, *J. Mater. Chem. A*, 2014, **2**, 14696.
53. H. Wei, S. Deng, B. Hu, Z. Chen, B. Wang, J. Huang and G. Yu, *ChemSusChem*, 2012, **5**, 2354.
54. A. Almasoudi and R. Mokaya, *J. Mater. Chem. A*, 2014, **2**, 10960.
55. J. A. Maciá-Agulló, B. C. Moore, D. Cazorla-Amorós and A. Linares-Solano, *Carbon*, 2004, **42**, 1367.
56. A. Almasoudi and R. Mokaya, *Micropor. Mesopor. Mater.*, 2014, **195**, 258.
57. A. Almasoudi and R. Mokaya. *J. Mater. Chem.*, 2012, **22**, 146.
58. M. Bbebu and C. Vasile, *Cellulose Chem. Technol*., 2010, **44**, 353.
59. H. Yang, R. Yan, H. Chen, C. Zheng, D. H. Lee and D. T. Liang, *Energy Fuels*, 2006**, 20***,* 388.

60. M. J. Antal, E. Croiset, X. Dai, C. DeAlmeida, W. S-L. Mok, N. Norberg, J-R. Richard and M. Al Majthoub, *Energy Fuels*, 1996, **10**, 652.
61. M. J. Antal, S. G. Allen, X. Dai, B. Shimizu, M. S. Tam and M. Gronli, *Ind. Eng. Chem. Res.*, 2000, **39**, 4024.
62. R. K. Sharma, J. B. Wooten, V. L Baliga, X. Lin, W. G. Chan and M. R. Hajaligol, *Fuel* 2004, **83**, 1469.
63. Z. Fang, T. Sato, R. L. Smith Jr, H. Inomata, K. Arai and J. A. Kozinski, *Biores. Technol.*, 2008, **99**, 3424.
64. W. M. A. W. Daud and W. S. W. Ali, *Bioresour. Technol*. 2004, **93**, 63.
65. G. Sethia and A. Sayari, *Carbon,* 2015, **93**, 68.
66. D. Lee, C. Zhang, C. Wei, B. L. Ashfeld and H. Gao, *J. Mater. Chem. A*, 2013, 1, 14862.
67. J. Silvestre-Albero, A. Wahby, A. Sepulveda-Escribano, M. Martinez-Escandell, K. Kaneko and F. Rodriguez-Reinoso, *Chem. Commun*., 2011, **47**, 6840.
68. G. Srinivas, J. Burress and T. Yildirim, *Energy Environ. Sci*., 2012, **5**, 6453.
69. M. Nandi, K. Okada, A. Dutta, A. Bhaumik, J. Maruyama, D. Derksa and H. Uyama, *Chem. Commun*., 2012, **48**, 10283.
70. Y. D. Xia, R. Mokaya, G. S. Walker and Y. Q. Zhu, *Adv. Energy Mater.*, 2011, **1**, 678.
71. A. Wahby, J. M. Ramos-Fernandez, M. Martnez-Escandell, A. Sepulveda-Escribano, J. Silvestre-Albero and F. Rodriguez-Reinoso, *ChemSusChem*, 2010, **3**, 974.
72. X. Fan, L. Zhang, G. Zhang, Z. Shu and J. Shi, *Carbon*, 2013, **61**, 423.
73. B. Smit, J. R. Reimer, C. M. Oldenburg and I. C. I. C. Bourg, *Introduction to Carbon Capture and Sequestration*, Imperial College Press, London, 1st edn, 2014.
74. G. T. Rochelle, *Science*, 2009, **325**, 1652.
75. D. Ko, R. Siriwardane and L. Biegler, *Ind. Eng. Chem. Res.* 2005, **44**, 8084.
76. E. S. Kikkinides, S. H. Cho and R. T. Yang, *Ind. Eng. Chem. Res.,* 1993, **32**, 2714.
77. L. Wang, Y. Yang, W. Shen, X. Kong, P. Li, J. Yu and A. E. Rodrigues, *Ind. Eng. Chem. Res.,* 2013, **52**, 7947.
78. J. M. Simmons, H. Wu, W. Zhou and T. Yildirim, *Energy Environ. Sci*., 2011, **4**, 2177.
79. Y. Belmabkhout, G. Pirngruber, E. Jolimaitre and A. Methivier, *Adsorption*, 2007, **13**, 341.
80. M. Beckner and A. Dailly, *J. Amer, Anal. Chem.* 2013, **4**, 8.
81. J. P. Marco-Lozar, M. Kunowsky, F. Suarez-Garcia, J. D. Carruthers and A. Linares-Solano, *Energy Environ. Sci*., 2012, **5**, 9833.

Graphical Abstract

Flash carbonization is an attractive yet simple route for the preparation of biomass (sawdust) derived carbons that exhibit attractive CO_2 uptake of up to 5.0 mmol g^{-1} (at 25 ^oC and 1 bar), and exceptional working capacity for pressure or vacuum swing adsorption process under simulated flue gas conditions.